Increased photosynthesis from a deep-shade to high-light regime occurs by enhanced CO_2 diffusion into the leaf of *Selaginella martensii*

Lorenzo Ferroni[a,b], Marián Brestič[b], Marek Živčak[b], Riccardo Cantelli[a], Simonetta Pancaldi[a]

[a] Department of Life Sciences and Biotechnology, University of Ferrara, Corso Ercole I d'Este 32, 44121 Ferrara, Italy

[b] Department of Plant Physiology, Slovak University of Agriculture, Tr. A. Hlinku 2, 949 01 Nitra, Slovakia

Authors of correspondence:

Lorenzo Ferroni

Department of Life Sciences and Biotechnology, University of Ferrara, C.so Ercole I d'Este 32, 44121 Ferrara, Italy

Email: lorenzo.ferroni@unife.it

Marián Brestič

Department of Plant Physiology, Slovak University of Agriculture, Nitra, A. Hlinku 2, 94976 Nitra, Slovak Republic

Email: marian.brestic@uniag.sk

ABSTRACT

The current understanding of photosynthesis across land plant phylogeny strongly indicates that ancient vascular plants are mainly limited by strong constitutive CO_2 diffusional constraints, particularly low stomatal and mesophyll conductance. Considering that the lycophyte *Selaginella martensii* can demonstrate long-term light acclimation, this study addresses the regulation extent of CO_2 assimilation in this species cultivated under contrasting light regimes of deep shade, medium shade and high light. Comparative analyses of photosynthetic traits, CO_2 conductance and leaf morpho-anatomy revealed acclimation plasticity similar to that of seed plants, though occurring in the context of an inherently low photosynthetic capacity typical of lycophytes. Specific modulations of the stomatal density and aperture, chloroplast surface exposed to mesophyll airspaces and cell wall thickness sustained a marked improvement in CO_2 diffusion from deep shade to high light. However, the maximum carboxylation rate was comparatively less effectively upregulated, leading to a greater incidence of biochemical limitations of photosynthesis. Because of a low carboxylation capacity under any light regime, a lycophyte prevents potential photodamage to the chloroplast by not only exploiting the thermal dissipation of excess absorbed energy but also diverting a large fraction of photosynthetic electrons to sinks alternative to carboxylation.

KEYWORDS

Selaginella martensii, lycophytes, photosynthetic acclimation, photosynthetic limitations

Abbreviations: α, leaf absorbance; β, partitioning of absorbed energy to PSII; Γ^*, CO_2 compensation point in the absence of day respiration; τ, α by β product; *A* and A_{max}, CO_2 assimilation and light-saturated CO_2 assimilation; C_a, reference CO_2 concentration; C_c, CO_2 concentration inside the chloroplast; C_i, intercellular CO_2 concentration; *F*, steady-state chlorophyll fluorescence; F_0, minimum chlorophyll fluorescence in the dark-acclimated state; F_M and F_M', maximum chlorophyll fluorescence in the dark- or light-acclimated state, respectively; F_V, variable chlorophyll fluorescence; f_{IAS}, fraction of leaf section occupied by intercellular airspaces; g_m, g_s and g_t, mesophyll, stomatal and total leaf CO_2 conductance, respectively; J_A, electron flow to alternative sinks; J_C and J_O, electron flow to carboxylation and oxygenation by RuBisCO, respectively; J_G, electron flow to photosynthesis and photorespiration; J_{max}, maximum electron flow for the regeneration of RuBP; J_{PSII}, total linear electron flow; *I* and I_{sat}, irradiance and saturating irradiance; *k*, apparent quantum yield of CO_2 fixation; K_C and K_O, catalytic constants of RuBisCO for the carboxylation and oxygenation activity, respectively; L, M and H, plants acclimated to deep shade, medium shade and high light, respectively; l_b, l_m and l_s, photosynthetic limitations due to biochemical constraints, mesophyll diffusional constraints, stomatal diffusional constraints, respectively; *Lc*, length of all chloroplast borders facing the airspace in a leaf section; *LCP*, light compensation point; *Lsec*, leaf section length; *NPQ*, non-photochemical quenching; *PQ*, photochemical capacity; PSI and PSII, photosystem I and II, respectively; *r*, ratio of CO_2 release per RuBisCO oxygenation; R_d, mitochondrial respiration; RuBP, ribulose-1,5-bisphosphate; *Sc/S*, chloroplast surface facing intercellular spaces ; T_{Chl}, chloroplast thickness; T_{CW}, cell wall thickness; V_{Cmax}, maximum velocity of carboxylation by RuBisCO; *Y(NO)*, *Y(NPQ)*, *Y(PSII)* quantum yields of non-regulatory energy dissipation, regulatory energy dissipation, and PSII photochemistry, respectively.

1. INTRODUCTION

Ferns and fern allies, traditionally called pteridophytes, share a generally much lower photosynthetic capacity than seed plants, especially angiosperms (Carriquí *et al*., 2015; Gago *et al*., 2019). This physiological feature is probably related to their evolutionary history. The appearance of most ancient pteridophytes is documented in the Silurian and Devonian periods (more than 400 Myr ago), when the atmospheric CO_2 concentration was 10-fold higher than today. The different selection pressures caused by atmospheric CO_2 are believed to have driven the respective evolution of pteridophytes and angiosperms, leading to a diversification of mechanisms for CO_2 diffusion and fixation, as suggested in a comparative study by Carriquí *et al*. (2015). They reported an average maximum rate of CO_2 fixation of 8 μmol CO_2 m^{-2} s^{-1} in ferns and fern allies, whereas the angiosperms sharing the same environment yielded ca. 19 μmol CO_2 m^{-2} s^{-1}.

Many causes contribute to the low carbon fixation capacity in pteridophytes. Their maximum velocity of carboxylation by RuBisCO (V_{Cmax}), maximum electron transport rates for the regeneration of RuBP (J_{max}), and CO_2 conductance are all lower than those in angiosperms (Carriquí *et al*., 2015). However, their photosynthetic capacity appears comparatively more limited by CO_2 diffusional constraints than by biochemical restrictions V_{Cmax} and J_{max} (Gago *et al*., 2013; Carriquí *et al*., 2015; Tosens *et al*., 2016; Veromann-Jürgenson *et al*., 2017; Xiong *et al*., 2018). Accordingly, some well-defined evolutionary trends were highlighted in leaf morpho-anatomy across vascular plant phylogeny (Gago *et al*., 2019). In leaves, the increase in stomatal conductance g_s parallels the gradual transition from the few large stomata observed in ferns to the high density of small stomata characterising angiosperms (Xiong *et al*., 2018). Likewise, the evolution of some specific anatomical features influenced non-stomatal CO_2 conductance (mesophyll conductance g_m *sensu lato*, considering that bryophytes lack a mesophyll; Carriquí *et al*., 2019), which expresses the facility of CO_2 diffusion through physico-chemical barriers from the substomatal cavities to RuBisCO inside the chloroplast stroma (Gago *et al*., 2019). From bryophytes to angiosperms, two phylogenetic trends have emerged in the anatomical traits of photosynthetic tissues: the cell wall thickness (T_{CW}) of photosynthetic cells

becomes increasingly thinner, and the chloroplast surface facing the intercellular spaces (S_c/S) progressively increases (Carriquí *et al*., 2015, 2019; Tosens *et al*., 2016; Veromann-Jürgenson *et al*., 2017, 2020; Gago *et al*., 2019). The most ancestral vascular plants, known as lycophytes, are deemed close to non-vascular bryophytes concerning photosynthetic physiology and some molecular mechanisms (Ferroni *et al*., 2016; Carriquí *et al*., 2019; Gerotto *et al*., 2019). In particular, their photosynthetic activity is largely limited by very low g_m due to thick mesophyll cell walls and small S_c/S (Tosens *et al*., 2016; Veromann-Jürgenson *et al*., 2017; Carriquí *et al*., 2019).

The phylogenetic position of lycophytes is extremely interesting because they are a sister group of all other vascular plants; instead, spermatophytes and all pteridophytes other than lycophytes belong to the monophyletic clade of euphyllophytes. Therefore, lycophytes, though spore-bearing vascular plants, are not close relatives of ferns but share with them an initial radiation under a high CO_2 atmosphere. The most distinctive morphological trait of lycophytes is their microphyll—i.e., a leaf with a single unbranched vein directly connected to the stem vascular bundle without a leaf gap (Banks, 2009). The extinction of most lycophytes down to the current 1% of extant tracheophytes suggests that the microphyll morphology was especially advantageous in a high CO_2 atmosphere (Beerling, 2005; Banks, 2009). Similar to bryophytes, the prevailing high CO_2 concentrations could explain the absence of an early selective pressure to develop thinner cell walls and higher S_c/S, in contrast to the subsequent emergence of flowering plants (Carriquí *et al*., 2019). Thick cell walls in mosses and liverworts are considered a constitutive trait of these lower plants, probably also associated with their poikilohydry and the consequent need for cells to tackle the mechanical stress of desiccation (Carriquí *et al*., 2019). Lycophytes are instead true vascular plants and regulate their water balance; until now, it is not known whether g_m and the related microphyll anatomical traits can be modulated in lycophytes as a developmental response to the environment.

With ca. 750 species, *Selaginella* is a cosmopolitan genus of lycophytes (Weststrand and Korall, 2016) that evolved some characteristics similar to those of euphyllophyte lineages independently (Banks, 2009). In recent years, some specificity of photosynthesis in lycophytes have emerged—for

example, investigating shade-adapted *Selaginella* species. The condition of monoplastidy in upper epidermal cells, a unique thylakoid architecture sub-differentiation, as well as chloroplast iridescence, are some unusual specialisations to deep-shade environments (Sheue *et al*., 2007, 2015; Masters *et al*., 2018; Liu *et al*., 2020). At the level of the thylakoid membrane, in the shade-adapted *S. martensii*, the short-term (minute scale) response to light includes a high capacity of antenna-based thermal dissipation of excess absorbed energy (non-photochemical quenching, *NPQ*) and photoprotective energy spill over from photosystem II (PSII) to photosystem I (PSI) (Ferroni *et al*., 2014, 2018). However, interesting is also the plant's ability to acclimate to light regimes as different as deep shade (low, far-red enriched irradiance) and full sunlight (high, full spectrum irradiance), with a marked gain in photochemical capacity in the high-light grown plants (Ferroni *et al*., 2016). In vascular plants, the shade-to-sun acclimation results from a complex combination of responses, not limited to thylakoid organisation, but including morpho-anatomical changes, which enhance the CO_2 supply and fixation (reviewed by Mathur *et al*., 2018). Compared with shade leaves, g_s increases in sun leaves mainly because of higher stomatal density but possibly also longer stomatal apertures (Lichtenthaler *et al*., 1981; Mathur *et al*., 2018; Harrison *et al*., 2019; Poorter *et al*., 2019); g_m is also positively regulated, especially increasing the mesophyll surface area faced by chloroplasts (Terashima *et al*., 2006). The strong CO_2 diffusional limitations affecting almost all ferns and fern allies analysed so far make it unclear whether the capacity of g_s and g_m can be effectively regulated in lycophytes in the long-term. Because the photosynthetic electron transport is upregulated in a sun regime in *S. martensii* (Ferroni *et al*., 2016), the plant would conceivably benefit from a parallel gain in g_s and g_m to ensure a sufficient CO_2 concentration at the carboxylation site of RuBisCO. Nevertheless, apparent minor regulation of *NPQ* capacity (Ferroni *et al*., 2016) indicates a limited electron sink capacity of the Calvin-Benson-Bassham cycle even in sun-acclimated plants. Based on the current understanding of photosynthetic limitations in ancestral land plants, *Selaginella* spp. included, this could mainly depend on strong constitutive CO_2 diffusional constraints (Carriquí *et al*., 2019; Gago *et al*., 2019). Therefore, this study aimed to contribute a response to the following questions in a lycophyte such as *S. martensii*: to what

extent is CO_2 assimilation regulated following acclimation to contrasting light regimes? Do lycophytes modulate leaf morpho-anatomical traits and what is the relative importance of the diffusional and biochemical limitations that ensue?

2. MATERIALS AND METHODS

2.1. Plant material and growth conditions

Clonal individuals of *Selaginella martensii* Spring (*Selaginellaceae*) were planted into pots in a warm humid greenhouse at the Botanical Garden of the University of Ferrara, where the air temperature is maintained at 25°C–30°C. Using plants grown under natural middle shade, three sub-sets of pots were exposed to stable natural light regimes according to Ferroni *et al*. (2016), allowing maximum photosynthetic photon flux densities of ca. 5, 50 and 1000 μmol m^{-2} s^{-1} at the middle of photoperiod for L, M and H plants, respectively, as monitored using a quantum-radiometer. Deep shade for L plants and medium shade for M plants were provided by the upper canopy in the greenhouse. Plants acclimated to different regimes in the period between April and July 2018 were sent to the Slovak University of Agriculture in Nitra, where they were placed in a greenhouse under similar conditions until gas exchange and fluorescence measurements were performed. Further plant sets were acclimated to L, M and H conditions in the greenhouse of Ferrara in August–September 2018 and used for microscopy.

2.2. Simultaneous gas exchange and chlorophyll florescence measurements

Analysis of photosynthetic parameters was based on simultaneous gas exchange and chlorophyll fluorescence emission in uncut terminal branches, i.e. ca. 2 cm-long stems including the first dichotomic ramification from the apex. An open infrared gas exchange system (Licor 6400, Licor, USA) was used. The terminal branches were carefully positioned in the measuring chamber side by side to completely cover the 2-cm^2 surface while avoiding as much as possible the overlapping of leaves. However, a partial overlapping of leaves belonging to the same branch and more evident in H plants

was unavoidable (Ferroni *et al.*, 2016). The leaf temperature was kept at 29°C, close to the environmental temperature of plant cultivation. The flow rate was set to 300 μmol s^{-1}, while the relative humidity was manually checked to be in the range of 60±5%.

To record the light-response curves of CO_2 assimilation (*A*), the reference CO_2 concentration was set to C_a=400 μmol mol^{-1} and the actinic light source was provided by the LED light unit of the system. After the branches were acclimated to darkness for 15 min inside the measuring chamber, the basal chlorophyll fluorescence F_0 was determined and a saturating pulse was applied to record the maximum fluorescence F_M and calculate the maximum PSII quantum yield by $F_V/F_M=(F_M-F_0)/F_M$. The subsequent measuring routine was started only in the case of $F_V/F_M \geq 0.760$, based on previous evaluation of normal values for this species. To allow stomatal opening and activation of the Calvin–Benson–Bassham cycle, the branches were first exposed to 200 (5 min) and 400 (10 min) μmol photons m^{-2} s^{-1}; given the sensitivity of stomatal opening to blue light in lycophytes (Doi *et al*., 2015), actinic light comprised 90% red and 10% blue. Subsequently, ten increasing irradiance steps were applied from 10 to 1200 μmol photons m^{-2} s^{-1}. Gas exchange and fluorescence measurements were performed regularly every 5 min, corresponding to steady-state conditions. The branches were kept in the chamber in the darkness for 10 min to allow the determination of dark respiration when the stomata were still open.

To obtain a response curve of *A* to the intercellular CO_2 concentration (C_i), the branches were positioned in the measuring chamber without previous dark acclimation. The branches were then exposed for 10 min to a saturating actinic light of 800 μmol photons m^{-2} s^{-1} (90% red and 10% blue) at a reference CO_2 concentration of 400 μmol mol^{-1} to activate photosynthesis and open the stomata to a stable level. The *A* value obtained at the end of this incubation was checked for consistency with *A* obtained from *A*-light curves under similar conditions to ascertain the healthy state of the branches under analysis. Subsequently, the samples were exposed to the following sequence of reference CO_2 concentrations under the same irradiance of 800 μmol photons m^{-2} s^{-1}: 300, 250, 200, 150, 100, 50, 400, 400, 600, 800, 1000, 1400, 1800, and 2200 μmol mol^{-1}. Each step lasted 2–4 min.

For both measuring routines (light and C_i curves), at the end of each step, a saturating pulse was applied to determine the steady-state fluorescence *F* and maximum fluorescence F_M' in the light-acclimated state, which were used to calculate the actual quantum yield of PSII $Y(PSII)=(F_M' - F)/ F_M'$ (Genty *et al*., 1989).

2.3. Assimilation curve fitting

The *A* values plotted against irradiance were fitted using an exponential Mitscherlich function and Origin version 2019b (OriginLab Corp., Northampton, MA, USA) (Peek*et al*., 2002; Heschel *et al*., 2004) (Eqn. 1):

$$A = A_{max}\left[1 - e^{-k(I-LCP)}\right]$$

where *I* is the incident irradiance, A_{max} is the upper asymptote corresponding to light-saturated *A*, *LCP* is the light compensation point, and *k* is the initial slope corresponding to the apparent quantum yield of CO_2 fixation. The irradiance of saturation was approximated resolving Eqn. 1 for $A= 0.95\ A_{max}$. Eqn. 1 was resolved for $I=0$ to obtain an acceptable approximate of the day mitochondrial respiration R_d, which was also checked for consistency with the values reported for *Selaginella* species by Carriquí *et al*. (2019).

To analyse A-C_i curves, the values of *A*, C_i and *Y(PSII)* were the input data for the Microsoft Excel™ utility developed by Moualeu-Ngangue, Chen and Stützel (2017). In this fitting procedure (hereafter MCS model), the A-C_i curve is treated according to the model of Farquhar, von Caemmerer and Berry (1980, FvCB model) to determine V_{Cmax} and J_{max} using the simultaneous changes in C_i-*Y(PSII)* to estimate the CO_2 concentration inside the chloroplasts (*Cc*) and g_m. The MCS model requires some entry constants: the CO_2 compensation point in the absence of day respiration Γ^*; the catalytic constants of RuBisCO for the carboxylation K_C and oxygenation K_O; and *O*, the air O_2 concentration (210 mmol mol^{-1}). Because no published values exist for Γ^*, K_C and K_O for *S. martensii* (or lycophytes in general), Γ^* was calculated as 40.38 at 29°C according to Long and Bernacchi (2003), while the K_C and K_O values reported in Moualeu-Ngangue *et al*. (2017) were used—i.e., K_C (404 μmol mol^{-1}) and K_O (278 μmol mol^{-1}). Such approximations could lead to imprecise absolute values of the relevant parameters;

however, they are acceptable to the comparative purpose of this work focusing on one single species under different light regimes. Nonetheless, the resulting parameter values were overall comparable to those in previous literature reports. Considering that *Selaginella* species can have very low V_{Cmax} (e.g., 13–17 μmol m^{-2} s^{-1} according to Carriquí *et al*., 2019), preliminary tests were performed on sample *A*-C_i curves recorded from *S. martensii* to roughly approximate V_{Cmax} from the initial *A*-C_i curve slope, which indicated a lower V_{Cmax} limit of ca. 20 μmol m^{-2} s^{-1}. Specific constraints to the calculation were then imposed in the MCS model to better match the specificity of *S. martensii*, particularly V_{Cmax} ≥20 μmol m^{-2} s^{-1} and J_{max} ≥20 μmol m^{-2} s^{-1}. To estimate g_m, the MCS model exploits the τ parameter, corresponding to the product of the leaf absorbance α by the partitioning β of energy between PSII and PSI. Although Moualeu-Ngangue *et al*. (2017) proposed to constrain τ in a boundary interval of 0.225<τ<0.57, a better fitting was obtained in *S. martensii* extending the upper limit to τ ≤0.70.

2.4. Analysis of photosynthetic limitations

The relative importance of stomatal l_s, mesophyll l_m and biochemical l_b limitations to photosynthesis was calculated according to Grassi and Magnani (2005) using the *A*, g_s, g_m values calculated from *A*-C_i-*Y(PSII)* data. The total CO_2 diffusion conductance was calculated as $g_t = 1/(1/g_s + 1/g_m)$, and the partition of photosynthesis limitations as follows (Eqn. 2–4):

$$l_s = \frac{\frac{g_t}{g_s} \times \frac{\partial A}{\partial C_c}}{g_t + \frac{\partial A}{\partial C_c}}$$

$$l_m = \frac{\frac{g_t}{g_m} \times \frac{\partial A}{\partial C_c}}{g_t + \frac{\partial A}{\partial C_c}}$$

$$l_b = \frac{g_t}{g_t + \frac{\partial A}{\partial C_c}}$$

The ratio $\partial A/\partial Cc$ was calculated following the FvCB model (Farquhar *et al*., 1980) (Eqn. 5):

$$\frac{\partial A}{\partial C_c} = V_{Cmax} \frac{\Gamma^* + K_C\left(1 + \frac{O}{K_O}\right)}{\left[C_c + K_C\left(1 + \frac{O}{K_O}\right)\right]^2}$$

2.5. Analysis of light energy partitioning and electron flows

Photosynthetic linear electron flow was calculated using fluorescence data obtained from *A*-light curves—i.e., under the constant C_a=400 μmol mol^{-1}. Fluorescence recorded at 400 μmol photons m^{-2} s^{-1} (corresponding to saturated *A* and available in duplicate for each curve) was used to calculate the PSII quantum yields according to Hendrickson *et al*. (2004), particularly the photochemical quantum yield [*Y(PSII)*], regulatory quantum yield [*Y(NPQ)*], and non-regulatory quantum yield [*Y(NO)*]. The photochemical capacity was estimated as *PQ=Y(PSII)/Y(NO)*, and the energy dissipation as Stern-Volmer-type non-photochemical quenching, *NPQ= Y(NPQ)/Y(NO)* (Lazár, 2015). The linear electron transport rate J_{PSII} was calculated as $J_{PSII} = I \times Y(PSII) \times \tau$. The τ average values obtained from the MCS model fitting of *A*-C_i curves were used, 0.65, 0.52 and 0.51 for L, M and H plants, respectively.

The available linear electron transport rate J_{PSII} was compared with the electron flux J_G required to support photosynthesis. J_G was calculated from CO_2 flux data using the following equation (Živčak *et al*., 2013) (Eqn. 6):

$$J_G = \frac{4(A + R_d)\left(Ci - \frac{A}{g_m} + \frac{\Gamma^*}{r}\right)}{Ci - \frac{A}{g_m} - \Gamma^*}$$

The average g_m values obtained from the MCS-modelled *A*-C_i-*Y(PSII)* curves were used for calculation: 0.0170, 0.0477, and 0.0625 mol CO_2 m^{-2} s^{-1} for L, M and H plants, respectively; *r* is the ratio of CO_2 release per RuBisCO oxygenation (=0.5). By comparison between J_{PSII} and J_G, the residual electron flow compared with the electrons available by PSII activity was calculated as the difference $J_A = J_{PSII} - J_G$ (Živčak *et al*., 2013).

Because J_G represents the net electron flow for the needs of RuBisCO, it was further dissected into the two electron flow components corresponding to electrons used due to RuBP carboxylation (J_C) or oxygenation (J_O), adapting the equations by Valentini *et al*. (1995) as follows (Eqn. 7-8):

$$J_C = \frac{1}{3}[J_G + 8(A + R_d)]$$

$$J_O = \frac{2}{3}[J_G - 4(A + R_d)]$$

2.6. Light and electron microscopy

Selaginella is an anisophyllous genus with dorsal and ventral (lateral) microphylls; in *S. martensii*, the latter are much larger than the former and were used for stomatal counting. Lateral microphylls were isolated from terminal branches, mounted in water on microslides and observed using a Zeiss Axiophot light microscope (Carl Zeiss, Oberkochen, Germany) under bright field with a 20× Zeiss Planapochromat objective.

For electron microscopy, small segments of the terminal branches were fixed with 3% glutaraldehyde in 0.1 M Na-cacodylate buffer (pH 7.2) for 3 h at 4°C and, after rinsing with the same buffer, they were post-fixed with 1% OsO_4 for 6 h at room temperature. The samples were then rinsed with 0.05 M Na-cacodylate buffer and dehydrated with an increasing acetone series. For scanning electron microscopy, the samples were critical-point dried and observed using a Zeiss EVO40 scanning electron microscope, which allows direct morphometric analyses during the observation. For transmission electron microscopy, after dehydration with acetone, the samples were instead treated with routine protocols for inclusion with Durcupan ACM epoxy resin. Ultrathin sections (80 nm) were obtained using an ultramicrotome, mounted on copper grids and stained with UranyLess® (Delta Microscopies, Mauressac, France) followed by lead citrate. Sections were observed using a Zeiss EM910 transmission electron microscope. Cell wall thickness (T_{cw}) was measured in the upper epidermal cells during the observation at a magnification of 50000×. Specifically, the cell wall portions interposed between chloroplast and mesophyll airspaces were analysed. From the same samples, semithin sections were also obtained, stained with toluidine blue for light microscopy and examined under a Zeiss Axiophot microscope with a 40× Zeiss Planapochromat objective. The chloroplast surface area per leaf area (S_C/S) was calculated following the method by Evans *et al*. (1994), with modifications related to the monoplastidy in the upper epidermal cells of the thin microphylls of *S. martensii*. In

detail, the length of all chloroplast borders facing the airspace (*Lc*) in the entire leaf section length (*Lsec*) available in each micrograph was measured using the segmented line tool of IMAGEJ freeware (Muir *et al*., 2014). S_C/S was approximated as the ratio *Lc/Lsec*. The fraction of leaf section occupied by intercellular airspaces (f_{IAS}) was also calculated, as well as the thickness of the chloroplast (Tc_{hl}).

2.7. Statistical analyses

The reported results of the photosynthetic parameters were expressed as the means of independent biological replicates as specified in the figures and tables for each analysis. The stomata were counted from 2 to 3 randomly sampled microphylls from different branches of 4–6 plants per acclimation type; stomatal morphometrics were measured from 3 to 5 microphylls of different plants during scanning electron microscopy observations; S_C/S and f_{IAS} were measured from 6-7 independent microphyll sections, in which T_{chl} was also determined for all upper epidermis chloroplasts; T_{cw} was determined from different microphylls observed with a transmission electron microscope. In all cases, the means were reported with standard errors. Multiple comparisons were performed by one-way analysis of variance (ANOVA) followed by Tukey's post hoc test, in both cases with a significance threshold of $P<0.05$. The Brown–Forsyth test for equal variance was run preliminarily using ANOVA; only in one case (J_A/J_{PSII}) was the condition of equal variance not met and the reported *P* value corresponded to the Brown–Forsythe *F** Test run with software Microsoft Excel™. All other statistical analyses were run with software Origin™ version 2020 (OrigiLab, Northampton, MA, USA), which was also used for graphing.

3. RESULTS

3.1. In *S. martensii*, the photosynthetic electron availability and carboxylation capacity increase along a light gradient

The light-response curves of chlorophyll fluorescence emission and gas exchange were first recorded to compare the photosynthetic capacity of *S. martensii* plants grown under extreme shade (L), intermediate shade (M), full sunlight (H). The main results are summarised in Table 1. The fluorescence-derived parameters under saturating light were largely comparable to those reported by Ferroni *et al*. (2016), confirming the homogeneity of the plant material with that analysed in previous research. In particular, the photochemical capacity *PQ* was strongly enhanced along the L-to-H gradient (ca. +170%) and not accompanied by significant changes in *NPQ* or *Y(NPQ)* (Ferroni *et al*., 2016). Likewise, modulation typical for shade/sun acclimation from L to H plants was evident from comparative light curves of CO_2 assimilation (Figure S1). The long-term photosynthetic acclimation in *S. martensii* involved expected changes in CO_2 fixation properties with increasing LCP, I_{sat} and A_{max}, along with decreasing CO_2 fixation quantum yield *k* (Heschel *et al*., 2004). Nonetheless, although A_{max} had increased in H plants, it remained very low in absolute terms—e.g., at the lower border for ferns and fern allies and consistent with values reported in *Selaginella* species, including *S. martensii* (Carriquí *et al*., 2015, 2019; Tosens *et al*., 2016).

[TABLE 1]

In *S. martensii*, a low photosynthetic capacity could depend on biochemical or CO_2 diffusional limitations. The biochemical constraints influencing a plant's photosynthetic capacity are the carboxylation activity and regeneration of the RuBP substrate. The former depends on the RuBisCO catalytic activity (in vivo carboxylation rate, V_{Cmax}) and reflects the concentration of the active enzyme in chloroplasts; the latter is instead allowed by the availability of electrons supplied by the photosynthetic electron transport chain initiated by PSII (maximum electron flow, J_{max}). The two parameters V_{Cmax} and J_{max} govern two subsequent rising phases in A-C_i curves (e.g., for a review, see

Long and Bernacchi, 2003). As shown in the examples in Figure 1A, a gradient in A-C_i curves was evident from L to H plants, and none of them reached a plateau, which excludes major limitations in triose-phosphate utilisation (Long and Bernacchi, 2003). The values of V_{Cmax} and J_{max} were obtained using the data fitting tool by Moualeu-Ngangue *et al*. (2017). As expected for an ancient vascular plant (Carriquí *et al*., 2015; Tosens *et al*., 2016), V_{Cmax} and J_{max} were low in *S. martensii* and both increased from L to H plants, as was predictable from the current knowledge of long-term acclimation to increasing light availability (Poorter *et al*., 2019). Because V_{Cmax} and J_{max} generally tend to change in parallel, the J_{max} $/V_{Cmax}$ ratio was expected to undergo marginal variations (Poorter *et al*., 2019). However, J_{max} $/V_{Cmax}$ actually increased significantly from L to M and H plants (Figure 1B). This latter observation indicated that, in lycophytes, the long-term acclimation from extreme shade (L) to medium shade (M) resulted in a greater maximum availability of electrons for RuBP regeneration (J_{max}) compared with the gain in RuBisCO activity (V_{Cmax}). Because the ~70% increase in A_{max} from L to M plants was not paralleled by a rise in V_{Cmax}, the former could have resulted instead from significant upregulation of the diffusional paths of CO_2 to RuBisCO.

[FIGURE 1 – 1 column fitting]

3.2. Following long-term light acclimation, *S. martensii* effectively regulates CO_2 diffusion from the atmosphere to chloroplasts

CO_2 diffusion from the atmosphere to RuBisCO is dependent on the contribution of g_s and g_m. The upregulation of g_s is a well-known component of shade-to-sun acclimation in angiosperms (Mathur *et al*., 2018; Poorter *et al*., 2019). The g_s values reported here for *S. martensii* were obtained from the gas fluxes recorded during the A-C_i curves; in particular, g_s at C_a=400 μmol mol^{-1}, representing a good approximation for light-saturated g_s (irradiance 800 μmol photons m^{-2} s^{-1}; Figure 2A). In *S. martensii* acclimated to deep shade, g_s was very low (g_s≈22 mmol CO_2 m^{-2} s^{-1}); however, a higher light availability

resulted in a strongly increased g_s, with a clear gradient from L to H plants, up to g_s≈50 mmol CO_2 m^{-2} s^{-1}—i.e., 130% higher in H than in L plants.

After CO_2 has entered the mesophyll airspaces, some diffusional barriers limit gas diffusion up to the catalytic site of RuBisCO inside the chloroplasts. To determine g_m, the MCS model was applied, in which g_m is estimated simultaneously with the biochemical parameters V_{Cmax} and J_{max} using τ (=$\alpha\times\beta$) as a key fitting parameter (Moualeu-Ngangue *et al*., 2017). The estimated τ values for good fitting of *S. martensii A-C_i-Y(PSII)* curves were quite high compared with the expected values in angiosperms but decreasing from 0.65 in L to 0.51 in H plants. In the study by Moualeu-Ngangue *et al*. (2017), the MCS model was meant to provide a means to evaluate g_m under varying C_i, an alternative to other methods that estimate average g_m from the entire *A*- C_i curve (Long and Bernacchi, 2003; Dubois *et al*., 2007; Carriquí et al., 2019). Examples of g_m- C_i curves obtained with *S. martensii* are shown in Figure S2. As advised by Moualeu-Nagungue *et al*. (2017), the model provides reliable g_m values only within a certain C_i range; in particular, it produces negative values at C_i<100 μmol mol^{-1}. In the case of *S. martensii*, starting from negative g_m estimates at very low C_i, there was an L-to-H gradient in the C_i-dependent increase in g_m, until positive values were reached for C_i≥200 μmol mol^{-1}. At C_i ≥700 μmol mol^{-1}, the model resulted in a drop to zero in g_m. Therefore, the range of reliable g_m was considered to be within C_i =200–700 μmol mol^{-1}, which well overlapped with that reported by Moualeu-Nagungue *et al*. (2017), indicating that the MCS method is reproducible in a species very distant from the model used for testing (*Cucumis sativus*). In the present study, the compared g_m values were obtained at 280< C_i<400 μmol mol^{-1}, where g_m was high and quite stable (Figure S2). In deep-shade acclimated *S. martensii*, the very low g_m (17 mmol CO_2 m^{-2} s^{-1}) was at the lower border of g_m variability in pteridophytes (Carriquí *et al*., 2015; Xiong *et al*., 2018). Very interestingly, g_m was strongly enhanced already in M plants (+180%), and even more in H plants (+260%) (Figure 2A). These results exclude a significant effect of reciprocal microphyll overlapping, which would have instead depressed g_m and g_s in H plants, where the degree of overlapping was the highest (Ferroni *et al.*, 2016). Because of the concomitant increase in g_m and g_s, the total conductance g_t underwent a steady increase from L to M (twofold) and H plants

(threefold) (Figure 2B). However, the g_m/g_s ratio indicated that the regulation of g_m prevailed over g_s at the L-to-M transition, while acclimation to H conditions occurred with a similar increment of both g_m and g_s (Figure 2A).

An enhancement of the CO_2 diffusional paths is expected to result in a higher CO_2 concentration available to RuBisCO inside the chloroplasts. In this respect, the effectiveness of the long-term g_t regulation was checked by comparing the C_C values calculated using the MCS model. Under conditions close to ambient CO_2 concentration (C_a=400 μmol mol^{-1}) or approaching maximum g_t (C_a≈600-800 μmol mol^{-1}), the comparative result was similar and revealed the effectiveness of upregulated g_t in increasing C_C, especially from L to M plants by 44%. Conversely, only a marginal gain in C_C occurred from M to H by 5%–7% (Figure 2C).

[FIGURE 2 – 1 column fitting]

3.3. Long-term regulation of the CO_2 diffusion capacity in *S. martensii* microphyll depends on the stomatal density and size, as well as on the chloroplast shape

In *S. martensii*, as in many other *Selaginella* species, the stomata were distributed in a band along the midrib at the underside of the ventral microphyll (Dengler, 1983; Figure S3). A few additional stomata were also found at the microphyll margin, a feature shared by several *Selaginella* species (Valdespino, 2015; Figure S3); because of their low number, the impact of marginal stomata on the overall g_s was considered minor, if at all (Younguang and Tan, 2013; Valdespino, 2015), and they were not included in the morphometric analyses. The stomatal density in the leaves of *S. martensii* L plants was very low—i.e., ca. 16 stomata mm^{-2}, but nearly doubled in H plants microphylls (Table 2; Figure 3A-C). In *S. martensii* microphylls, the stomata were very small, especially compared with the large stomata typically found in pteridophytes (e.g., Xiong *et al*., 2018). However, along the L-to-H gradient, the stomatal size increased by 40% and, correspondingly, the stomatal aperture became longer by 26% (Table 2; Figure 3D-F). It was hypothesised that the increase in g_s, which was measured on an area

basis, could be due to combined increases in the stomatal density and aperture. An estimate of the total stomatal aperture length on an area basis (i.e., stomata number mm^{-2} × aperture length) perfectly matched the 130% increase in g_s occurring in H plants. Therefore, in *S. martensii*, an efficient long-term regulation of g_s capacity along the L-to-H light was achieved by increasing the overall length of stomatal apertures.

[FIGURE 3 – 2 column fitting]

[TABLE 2]

The capacity for g_m is dependent on the morpho-anatomical traits of a leaf that are mainly governed by the chloroplast surface area exposed to intercellular air spaces (S_C/S) and cell wall thickness (T_{cw}) (Gago *et al*., 2019). In the microphyll of *S. martensii*, as in many other *Selaginella* species, the tissues are organised into three cell layers, all bearing chloroplasts: large conical upper epidermal cells, few sparse lobed mesophyll cells, and flat lower epidermal cells (Figure 3G). The giant cup-shaped chloroplast at the bottom of each cell of the upper epidermis is responsible for most of the photosynthetic activity in *Selaginella* leaves. In the other two layers, cells contain some lens-shaped chloroplasts. Along the L-to-H light gradient, f_{IAS} did not undergo significant changes. However, conversely, S_C/S increased progressively and markedly; in fact, H plants had a twofold S_C/S increase compared with L plants (Table 3). The cause for such an increment was easily attributable to a progressively more definite concavity of the chloroplast in upper epidermal cells (Figure 3G-I). T_{cw} was measured in the upper epidermal cells at positions where the chloroplast faced the mesophyll airspaces. The already thin cell wall, <180 nm in L plants, became even thinner, though slightly, in plants grown with a higher availability of light (Table 3; Figure 3J-L). As an additional factor potentially influencing g_m, T_{chl} was also measured, but there was no gradient from L to H plants; in H plants, T_{chl} was actually intermediate between L and M plants (Table 3).

[TABLE 3]

3.4. In *S. martensii* H plants, photosynthesis is mainly limited by biochemical constraints

To evaluate the relative importance of diffusional and biochemical factors in the *S. martensii* photosynthetic capacity, the photosynthetic limitations were compared (Figure 4). In L plants, the three components l_s, l_m, and l_b influenced photosynthesis similarly, with a relatively dominant limitation due to CO_2 mesophyll diffusion (ca. 40%). The long-term acclimation of photosynthesis from the L to M condition strongly affected the importance of l_m and l_b, involving a decreased importance of limitations linked to CO_2 diffusion inside the mesophyll. Interestingly, the long-term regulation in H plants allowed the specific weight of each limitation to be unvaried compared with that in M plants. Therefore, in M and H plants, photosynthesis was mainly limited by biochemical constraints (nearly 50%).

[FIGURE 4 – 1 column fitting]

3.5. Electron flow to alternative sinks is very active in *S. martensii*

At the transition from extreme shade to higher light availability, the discrepancy between increased PQ, J_{max}, g_t and, conversely, stable V_{Cmax} suggested that *S. martensii* could have a certain flexibility in the management of electrons made available by PSII, but only partly usable for CO_2 fixation. Therefore, the partition of photosynthetic electrons into the fluxes driven to RuBP carboxylation or oxygenation, or to alternative electron sinks was analysed. The calculations refer to values obtained from light-*A* curves at a saturating light of 400 µmol photons m^{-2} s^{-1} (Figure S3) and use estimates of τ and g_m from the MCS model.

After correction for the estimated τ, J_{PSII} was still consistent with the results obtained from *Y(PSII)* and doubled from L to H plants (Figure 5A). These electrons can be used downstream of RuBisCO to allow the regeneration of compounds in the Calvin–Benson–Bassham cycle (J_C) or in the

photorespiratory pathway (J_O). In *S. martensii*, the partitioning analysis of photosynthetic electrons revealed a parallel increase in J_C and J_O along the L-M-H gradient and their ratio was invariable (Figure 5B, C). The electrons produced in excess of the RuBisCO needs (J_C+J_O) are funnelled to "alternative electron sinks" (J_A). Although not statistically significant, an increasing trend of J_A was also visible (Figure 5B); the relative importance of J_A compared with the total linear flux J_{PSII} did not undergo significant changes between plants (Figure 5D). Importantly, under each condition of long-term acclimation, J_A accounted for 30%–45% of J_{PSII} (Figure 5D).

[FIGURE 5 – 2 column fitting]

4. DISCUSSION

Lycophytes, though true vascular plants, are often considered an intermediate evolutionary step between bryophytes (mosses, liverworts) and euphyllophytes (ferns and seed plants). Their photosynthetic rates are higher than those of bryophytes but still very low compared with that of their sister group of euphyllophytes (Carriquí *et al*., 2015, 2019). This study demonstrated that their carbon fixation depends strongly on the light environment of growth, which induces wide modulations of the CO_2 conductance in the microphyll, with a dynamic range unexpectedly comparable to that of seed plants.

The parameters obtained in this work partially overlap with the corresponding variability ranges of means recently reported by Carriquí *et al*. (2019) for three *Selaginella* species (Figure S4). However, some divergence was expected—e.g., because of the higher temperature chosen for photosynthesis measurements—as demonstrated by the higher V_{Cmax}. For a tropical species routinely cultivated indoors at 25°C–30°C, our V_{Cmax} result is consistent with a temperature closer to the optimum (29°C instead of 20°C–22°C in Carriquí *et al*., 2019; see also Leuning, 2002). However, V_{Cmax} in a lycophyte remains inherently low—i.e., lower than average typical values in euphyllophytes, either ferns or angiosperms (ca. 40 *vs* 100 or 143 μmol CO_2 m^{-2} s^{-1}, respectively, according to Carriquí *et al*., 2015).

Another element possibly leading to discrepancies can be the use of the fitting model of *A-C_i-Y(PSII)* curves recently developed by Moualeu-Ngangue *et al*. (2017), whose most important novelty is the estimation of the τ parameter incorporated in the algorithm. In the common routine, τ is often approximated as 0.42, assuming that 84% of light energy is absorbed by a typical leaf and excitation energy is evenly distributed between PSI and PSII (for short review, see Kalaji *et al*., 2017, pp. 23-26). Interestingly, in *S. martensii*, high τ values well matched the great abundance of LHCII potentially serving PSII previously reported in this species under any condition of long-term light acclimation, a feature that is also mirrored by a high stacking degree of thylakoids (Ferroni *et al*., 2016). Additionally, the highest τ in extreme shade plants agrees with their low PSI relative content (Ferroni *et al*., 2016). Understorey plants experience a very low irradiance enriched in far-red light, making the photosystem stoichiometry change in favour of PSII (Lichtenthaler and Babani, 2004).

Despite any possible bias derived from the model and approximations, the resulting parameters reveal very meaningful gradients following *S. martensii* acclimation to contrasting light environments. The basic regulatory mechanisms subtended to long-term light acclimation are well known in angiosperms (Mathur *et al*., 2018; Poorter *et al*., 2019). However, they are probably shared by all vascular plants, possibly inherited from a common ancestor (Sello *et al*., 2019). In *S. martensii*, the overall direction of long-term changes is indeed the same as that in angiosperms, despite a low efficiency of CO_2 fixation. Similar to ferns, in lycophytes, CO_2 assimilation is mainly limited by l_m (Tosens *et al*., 2016; Veromann-Jürgenson *et al*., 2017; Carriquí *et al*., 2019; Gago *et al*., 2019); however, our results highlight an unexpectedly strong effect of the growth light regime on conductance capacities. Compared with that in L plants, the relative importance of photosynthesis limitations in M and H plants becomes closer to that in angiosperms, which are more limited by biochemical than diffusional factors (Muir *et al*., 2014; Carriquí *et al*., 2015; Gago *et al*., 2019). In particular, the L-to-M transition reveals some unique features in lycophytes. For example, g_s and g_m should change in parallel to each other to supply RuBisCO with CO_2; however, the increase in g_m largely exceeds that of g_s. The consequent ability

of *S. martensii* to keep l_s constant and even markedly decrease l_m along the light regime gradient depends on clear developmental changes in microphyll morpho-anatomy.

In recent years, lycophytes have represented an interesting plant material to investigate stomatal opening mechanics, which are probably similar to those operating in the first vascular plants (Doi *et al*., 2015; Brodribb *et al*., 2019). However, stomata also undergo developmental regulation influencing their size, density and patterning on the leaf surface (Harrison *et al*., 2019). The results obtained in angiosperms following changes in CO_2 supply or in mutants indicate that the size and density of stomata are regulated towards opposite directions to accomplish the requirements of the cost-benefit balance and spatial constraints in the epidermis (de Boer *et al*., 2016; Harrison *et al*., 2019). In particular, in angiosperms, a higher efficiency in g_s responsiveness is achieved by differentiating smaller and denser stomata, which is an expensive solution for the plant and can be compatible only with high photosynthetic rates (Harrison *et al*., 2019). This physiological statement finds an interesting evolutionary confirmation across the euphyllophyte lineage; the transition from sparse large stomata in ferns to dense small stomata in angiosperms parallels a corresponding increase in photosynthetic capacity (Carriquí *et al*., 2015; Xiong *et al*., 2018). However, *S. martensii* seems to deviate from this evolutionary trend: the stomata, which cluster in a band, are collectively not dense but are as small as those in monocots (Xiong *et al*., 2018). These features can presumably offer an advantage in deep shade environments (see the case of *Begonia plebeja* reported by Papanatsiou *et al*., 2017). Nevertheless, *S. martensii* can successfully acclimate to a sun regime with respect to stomatal features. In angiosperms, the long-term light regulation of g_s seems to depend primarily on stomatal density (Poorter *et al*., 2019). In *S. martensii*, the optimisation of g_s occurs through concerted adjustments of both stomatal density and size, without changing the typical patterning in the *Selaginella* genus.

In parallel to increasing g_s capacity, other changes in *S. martensii* microphyll architecture occur to ensure sufficient C_C at the RuBisCO site. Although g_m is a multifactorial property, current research convincingly converges to only two fundamental leaf anatomical determinants with specific

importance phylogenetically—i.e., T_{cw} and *Sc/S* (Carriquí *et al*., 2015, 2019; Tosens *et al*., 2016; Veromann-Jürgenson *et al*., 2017, 2020). Across plant evolution, these two parameters are negatively related; the inference was that lycophytes, such as *Selaginella* or *Lycopodium*, have low g_m owing to their thick cell walls and small *Sc/S* (Tosens *et al*., 2016; Veromann-Jürgenson *et al*., 2017; Carriquí *et al*., 2019; Gago *et al*., 2019). In our plants, T_{cw}<200 nm was measured in contrast to T_{cw}≈500 nm reported by Carriquí *et al*. (2019) in the same species. A similar discrepancy can be found for *S. uncinata*, in which T_{cw} was 200 nm in Veromann-Jürgenson *et al*. (2017) but 500 nm in Carriquí *et al*. (2019). Thus, in addition to evolutionary arguments, T_{cw} may change between different ecotypes and, as shown herein, may be significantly influenced by environmental factors. However, although g_m involves variations in both T_{cw} and *Sc/S*, the modulability of the latter appears more decisive following long-term acclimation in *S. martensii* and is related to changes in chloroplast shape. The single giant chloroplast hosted in the upper epidermal cells undoubtedly offers an advantage to light harvesting in deep shade (Sheue *et al*., 2007, 2015; Liu *et al*., 2020); however, it can also undergo some relevant variations to cope with a sun regime (Sheue *et al*., 2015; Ferroni *et al*., 2016). In particular, the regulation of chloroplast concavity strongly influences the efficiency of CO_2 supply to RuBisCO, leading to the striking increase in g_m at the transition from the L to M regime. By comparison, under M and H light conditions, g_m is somewhat higher than expected for a lycophyte (Carriquí *et al*., 2019; Figure S4).

The range of J_{max}/V_{Cmax} variation in *S. martensii* agrees with results reported by Tosens *et al*. (2016) in a comparative study on 35 species of ferns and fern allies; however, we show that J_{max}/V_{Cmax} in lycophytes is modulated based on the light regime. A recent meta-analysis by Poorter *et al*. (2019) highlighted that J_{max}/V_{Cmax} is an almost invariable trait in seed plants following long-term light acclimation, indicating that the coordinated regulation of plastid- and nuclear-encoded genes specifically ensures the constancy of the ratio (Poorter *et al*., 2019). A strong relationship between J_{max} and V_{Cmax} is deemed a fundamental feature of the photosynthetic system across species and environments because it would be required to prevent photoinhibition under saturating light (Walker *et al*., 2014). Thus, under deep shade, the constraints on J_{max}/V_{Cmax} likely become less stringent, owing

to the low probability for the plant to be exposed to saturating light, whereas survival depends instead on powerful investments in light harvesting. Accordingly, the lowest J_{max}/V_{Cmax} in *S. martensii* L plants suggests a lesser investment in electron transport capacity for RuBP regeneration than RuBisCO activity. It is noteworthy that the electron availability under saturating light still exceeds the carboxylation capacity. Exceeding electron availability over the photosynthetic needs appears to be a characteristic feature in *S. martensii* under all light regimes. When electrons are produced in excess of the RuBisCO carboxylation capacity, relief from an over-reduced state of the stroma electron carriers can involve modified electron use. Photorespiration is considered the major alternative sink of electrons in all C3 land plants, where it cooperates with the safe accumulation of oxidised PSI (Hanawa *et al*., 2017; Shimakawa and Miyake, 2018; Huang *et al*., 2019). While this role is conceivably played by photorespiration also in *S. martensii*, its relative importance does not change following long-term light acclimation, leading to constant J_O/J_C. Beyond photorespiration, other alternative sinks are responsible for discrepancies between electron availability (as J_{PSII}) and electrons accepted by RuBisCO-initiated pathways (as J_G; Živčak *et al*., 2013). Such alternative fluxes are collectively represented by J_A and include safety valves based on electron funnelling to O_2 reduction, particularly through the "water-water cycle" and the chlororespiratory pathway (reviewed by Alric and Johnson, 2017). In *S. martensii*, the amount of electrons potentially divertible to J_A is high, reaching even more than 40% of J_{PSII}. The long-term upregulation of J_{PSII} from L to H plants is accompanied by a parallel increase in J_A, whose biochemical effectors could be the flavodiiron proteins involved in the water-water cycle in lycophytes (Ilík *et al*., 2017) or the NAD(P)H dehydrogenase (NDH)-plastid terminal oxidase (PTOX) system for chlororespiratory electron recycling to O_2 (Peltier *et al*., 2016). A striking accumulation of NDH was previously reported in high-light-grown *S. martensii* (Ferroni *et al*., 2016). However, intriguingly, even deep-shade *S. martensii* preserves a relatively high potential for J_A, despite having been acclimated to an irradiance hardly reaching the *LCP*. Current research concerning the potential of understorey plants to cope with light flecks has revealed different facets of a very complex problem (e.g., Demmig-Adams *et al*., 2015; Sun *et al*., 2020). Our observations in a lycophyte suggest that J_A may be crucial for the

initial land colonisation in early vascular plants to survive, not just excess light but rather the unpredictable changes in irradiance occurring in increasingly complex land plant consortia.

Poorter *et al*. (2019) have recently reviewed the literature on seed plant responses to the daily light integral, determining for each of 70 traits a plasticity index. Because of many morphological, physiological and biochemical features, *S. martensii* can be defined as a shade-tolerant species and should have a low acclimation plasticity (Poorter *et al*., 2019). However, we show that a lycophyte such as *S. martensii* reveals a phenotypic plasticity of photosynthesis to contrasting light regimes that is *very close to that of seed plants* (Table 4). For some years, many research contributions have stressed the importance of constrained CO_2 diffusion as a main and constitutive cause for low photosynthesis in ancient vascular plants (reviewed in Gago *et al*., 2019). We show that, in *S. martensii*, the effectiveness of CO_2 diffusion is instead well regulated based on the growth light environment and is sustained by specific modulations of the microphyll morpho-anatomy. However, even if CO_2 diffusion from the atmosphere to the mesophyll can be remarkably enhanced in high-light-acclimated plants, their photosynthesis remains low because of emerging biochemical limitations; V_{Cmax} is indeed less plastic than parameters related to electron transport or CO_2 diffusion. Consequently, photosynthesis is soon saturated, explaining why the plant has a high *NPQ* capacity (Ferroni *et al*., 2014, 2016, 2018) and exploits also mechanisms to remove the many electrons that still cannot be used for CO_2 fixation.

[TABLE 4]

ACKWNOLEDGEMENTS

This research was funded by the Slovak Academic Information Agency (scholarship granted to L.F.), the University of Ferrara (FAR2018 granted to L.F. and to S.P.), EPPN2020-OPVaI-VA - ITMS 313010T813 (granted to M.B.). The authors thank Fausto Molinari (Botanical Garden of the University of Ferrara) and Jana Ferencová (Dept. of Plant Physiology, Slovak University of Agriculture in Nitra) for their help in plant establishment and maintenance; Paola Boldrini (Electron Microscopy Centre, University of Ferrara) for excellent technical assistance in electron microscopy; Alex Zeri for valuable help in collecting morphometric data.

CONFLICT OF INTEREST

The authors declare no conflict of interest.

AUTHOR CONTRIBUTION

L.F. conceived and designed the study and performed the experiments; M.B. and M.Z provided analytical tools and supported results interpretation; L.F. and R.C. analysed the data; L.F. wrote the manuscript; S.P. and M.B. critically revised the manuscript for important intellectual content.

DATA AVAILABILITY

Raw data are available upon request from the authors.

LEGENDS FOR SUPPLEMENTARY INFORMATION

Supplementary Figure 1. Net CO_2 assimilation as a function of irradiance in *Selaginella martensii* acclimated to extreme shade (L), medium shade (M), and high-light (H) natural regime.

Supplementary Figure 2. Examples of the variation in the estimated mesophyll conductance (g_m) with the intercellular CO_2 concentration (C_i) in the leaves of *Selaginella martensii* long-term acclimated to extreme shade (L), medium shade (M) and high-light (H) natural regimes.

Supplementary Figure 3. Scanning electron micrographs of *Selaginella martensii* microphylls in plants long-term acclimated to extreme shade, middle shade and high-light regime.

Supplementary Figure 4. Parameters related to the photosynthetic performance obtained in *Selaginella martensii* under the three conditions of long-term light acclimation (L, extreme shade; M, medium shade; H, high light) compared with values obtained from *Selaginella* species by Carriquí *et al*. (2019).

REFERENCES

Alric J. and Johnson X. (2017) Alternative electron transport pathways in photosynthesis: a confluence of regulation. *Current Opinion in Plant Biology* 37, 78–86.

Banks J.A. (2009) Selaginella and 400 million years of separation. *Annual Review of Plant Biology* 60, 223–38.

Beerling D.J. (2005) Leaf evolution: gases, genes and geochemistry. *Annals of Botany* 96, 345–352.

de Boer H. J., Price C.A., Wagner-Cremer F., Dekker S. C., Franks P. J. and Veneklaas E.J. (2016) Optimal allocation of leaf epidermal area for gas exchange. *New Phytologist* 210, 1219–1228.

Brodribb T. J., Sussmilch F. and McAdam S. A. M. (2019) From reproduction to production, stomata are the master regulators. *The Plant Journal* 101, 756-767.

Carriquí M., Cabrera H. M., Conesa M. À., Coopman R. E., Douthe C., Gago J., Gallé A., Galmés J., Ribas-Carbo M., Tomás M. and Flexas J. (2015) Diffusional limitations explain the lower photosynthetic capacity of ferns as compared with angiosperms in a common garden study. *Plant, Cell and Environment* 38, 448–460.

Carriquí M., Roig-Oliver M., Brodribb T. J., Coopman R. E., Gill W., Mark K., Niinemets Ü., Perera-Castro A. V., Ribas-Carbo M., Sack L., Tosens T., Waite M. and Flexas J. (2019) Anatomical constraints to nonstomatal diffusion conductance and photosynthesis in lycophytes and bryophytes. *New Phytologist* 222, 1256–1270.

Dengler N. G. (1983) The developmental basis of anisophylly in *Selaginella martensii*. II. Histogenesis. *American Journal of Botany* 70, 193-206.

Demmig-Adams B., Muller O., Stewart J. J., Cohu C. M. and Adams III W. (2015) Chloroplast thylakoid structure in evergreen leaves employing strong thermal energy dissipation. *Journal of Photochemistry and Photobiology B: Biology* 152, 357-366.

Doi M., Kitagawa Y. and Shimazaki K. (2015) Stomatal blue light response is present in early vascular plants. *Plant Physiology* 169, 1205–1213.

Dubois J. J., Fiscus E. L., Booker F. L., Flowers M. D. and Reid C. D. (2007) Optimizing the statistical estimation of the parameters of the Farquhar–von Caemmerer-Berry model of photosynthesis. *New Phytologist* 176, 402–414.

Evans J.R., von Caemmerer S., Setchell B.A. and Hudson G.S. (1994) The relationship between CO_2 transfer conductance and leaf anatomy in transgenic tobacco with a reduced content of Rubisco. *Australian Journal of Plant Physiology* 21, 475–495.

Farquhar G. D., von Caemmerer S. and Berry J. A. (1980) A biochemical model of photosynthetic CO_2 assimilation in leaves of C3 species. *Planta* 149, 78–90.

Ferroni L., Angeleri M., Pantaleoni L., Pagliano C., Longoni P., Marsano F., Aro E.-M., Suorsa M., Baldisserotto C., Giovanardi M., Cella R. and Pancaldi S. (2014). Light dependent reversible phosphorylation of the minor photosystem II antenna Lhcb6 (CP24) occurs in lycophytes. *The Plant Journal* 77, 893–905.

Ferroni L., Suorsa M., Aro E.-M., Baldisserotto C. and Pancaldi S. (2016) Light acclimation in the lycophyte *Selaginella martensii* depends on changes in the amount of photosystems and on the flexibility of the light-harvesting complex II antenna association with both photosystems. *New Phytologist* 211, 554–568.

Ferroni L., Cucuzza S., Angeleri M., Aro E.-M., Pagliano C., Giovanardi M., Baldisserotto C. and Pancaldi S. (2018) In the lycophyte *Selaginella martensii* is the “extra-qT” related to energy spillover? Insights into photoprotection in ancestral vascular plants. *Environmental and Experimental Botany* 154, 110–122.

Gago J., Coopman R. E., Cabrera H. M., Hermida C., Molins A., Conesa M. A., Galmés J., Ribas-Carbó M. and Flexas J. (2013) Photosynthesis limitations in three fern species. *Physiologia Plantarum* 149, 599–611.

Gago J., Carriquí M., Nadal M., Clemente-Moreno M. J., Coopman R. E., Fernie A. R. and Flexas J. (2019) Photosynthesis optimized across land plant phylogeny. *Trends in Plant Science* 24, 947-958.

Genty B., Briantais J.-M. and Baker N. R. (1989) The relationship between the quantum yield of photosynthetic electron transport and quenching of chlorophyll fluorescence. *Biochimica et Biophysica Acta* 990, 87–92.

Gerotto C., Trotta A., Bajwa A.A., Mancini I., Morosinotto T. and Aro E.-M. (2019) Thylakoid Protein Phosphorylation Dynamics in a Moss Mutant Lacking SERINE/THREONINE PROTEIN KINASE STN8. *Plant Physiology* 180, 1582–1597.

Grassi G. and Magnani F. (2005) Stomatal, mesophyll conductance and biochemical limitations to photosynthesis as affected by drought and leaf ontogeny in ash and oak trees. *Plant, Cell and Environment* 28, 834–849.

Hanawa H., Ishizaki K., Nohira K., Takagi D., Shimakawa G., Sejima T., Shaku K., Makino A and Miyake C. (2017) Land plants drive photorespiration as higher electron-sink: comparative study of post-illumination transient O_2-uptake rates from liverworts to angiosperms through ferns and gymnosperms. *Physiologia Plantarum* 161, 138–149.

Harrison E. L., Cubas L. A., Gray J. E. and Hepworth C (2019) The influence of stomatal morphology and distribution on photosynthetic gas exchange. *The Plant Journal* 101, 768–779.

Hendrickson L., Furbank R. T. and Chow W. S. (2004) A simple alternative approach to assessing the fate of absorbed light energy using chlorophyll fluorescence. *Photosynthesis Research* 82, 73–81.

Heschel M. S., Stinchcombe J. R., Holsinger K. E. and Schmitt J. (2004) Natural selection on light response curve parameters in the herbaceous annual, *Impatiens capensis*. *Oecologia* 139, 487-494.

Huang W., Yang Y.-J., Wang J.-H. and Hu H. (2019) Photorespiration is the major alternative electron sink under high light in alpine evergreen sclerophyllous *Rhododendron* species. *Plant Science* 289, 110275.

Ilík P., Pavlovič A., Kouřil R., Alboresi A., Morosinotto T., Allahverdiyeva Y., Aro E.-M., Yamamoto H. and Shikanai T. (2017) Alternative electron transport mediated by flavodiiron proteins is operational in organisms from cyanobacteria up to gymnosperms. *New Phytologist* 214, 967–972.

Kalaji H. M., Schansker G., Brestič M., Bussotti F., Calatayud A., Ferroni L., Goltsev V., Guidi L., Jajoo A., Li P., Losciale P., Mishra V. K., Misra A. N., Nebauer S. G., Pancaldi S., Penella C., Pollastrini M., Suresh K., Tambussi E., Yanniccari M., Živčak M., Cetner M. G., Samborska I. A., Stirbet A., Olsovska K., Kunderlikova K., Shelonzek H., Rusinowski A. and Baba W. (2017) Frequently asked questions about chlorophyll fluorescence, the sequel. *Photosynthesis Research* 132, 13–66.

Lazár D. (2015) Parameters of photosynthetic energy partitioning. *Journal of Plant Physiology* 175, 131–147.

Leuning R. (2002) Temperature dependence of two parameters in a photosynthesis model. *Plant, Cell and Environment* 25, 1205–1210.

Lichtenthaler H. K. and Babani F. (2004) Light adaptation and senescence of the photosynthetic apparatus. Changes in pigment composition, chlorophyll fluorescence parameters and photosynthetic activity. In Chlorophyll a fluorescence a signature of photosynthesis – advances in photosynthesis and respiration series, vol. 19 (eds G.C. Papageorgiou and Govindjee), pp. 713–736. Springer, Dordrecht - the Netherlands.

Lichtenthaler H. K., Buschmann C., Döll M., Fietz H. J., Bach T., Kozel U., Meier D. and Rahmsdorf U. (1981) Photosynthetic activity, chloroplast ultrastructure, and leaf characteristics of high-light and low-light plants and of sun and shade leaves. *Photosynthesis Research* 2, 115-141.

Liu J. W., Li S. F., Wu C. T., Valdespino I. A., Ho J. F., Wu Y. H., Chang H. M., Guu T. Y., Kao M. F., Chesson C., Das S., Oppenheimer H., Bakutis A., Saenger P., Allen N. S., Yong J. W. H., Adjie B., Kiew R., Nadkarni N., Huang C. L., Chesson P. and Sheue C. R. (2020) Gigantic chloroplasts, including bizonoplasts, are common in shade-adapted species of the ancient vascular plant family Selaginellaceae. *American Journal of Botany* 107, 1–15.

Long S.P. and Bernacchi C. J. (2003) Gas exchange measurements, what can they tell us about the underlying limitations to photosynthesis? Procedures and sources of error. *Journal of Experimental Botany* 54, 2393–2401.

Masters N. J., Lopez-Garcia M., Oulton R. and Whitney H. M. (2018) Characterization of chloroplast iridescence in *Selaginella erythropus*. *Journal of the Royal Society Interface* 15, 20180559.

Mathur S., Jain L. and Jajoo A. (2018) Photosynthetic efficiency in sun and shade plants. *Photosynthetica* 56, 354-365.

Moualeu-Ngangue D. P., Chen T.-W. and Stützel H. (2017) A new method to estimate photosynthetic parameters through net assimilation rate-intercellular space CO_2 concentration (A-C_i) curve and chlorophyll fluorescence measurements. *New Phytologist* 213, 1543–1554.

Muir C. D., Hangarter R. P., Moyle L. C. and Davis P. A. (2014) Morphological and anatomical determinants of mesophyll conductance in wild relatives of tomato (*Solanum* sect. *Lycopersicon*, sect. *Lycopersicoides*; Solanaceae). *Plant, Cell and Environment* 37, 1415–1426.

Papanatsiou M., Amtmann A. and Blatt M.R. (2017) Stomatal clustering in *Begonia* associates with the kinetics of leaf gaseous exchange and influences water use efficiency. *Journal of Experimental Botany* 68, 2309–2315.

Peek M.S., Russek-Cohen E., Wait D.A. and Forseth I.N. (2002) Physiological response curve analysis using nonlinear mixed models. *Oecologia* 132, 175–180.

Peltier G., Aro E.-M. and Shikanai T. (2016) NDH-1 and NDH-2 plastoquinone reductases in oxygenic photosynthesis. *Annual Review of Plant Biology* 67, 55-80.

Poorter H., Niinemets Ü., Ntagkas N., Siebenkäs A., Mäenpää M., Matsubara S. and Pons T. L. (2019) A meta-analysis of plant responses to light intensity for 70 traits ranging from molecules to whole plant performance. *New Phytologist* 223, 1073-1105.

Sello S., Meneghesso A., Alboresi A., Baldan B. and Morosinotto T. (2019) Plant biodiversity and regulation of photosynthesis in the natural environment. *Planta* 249, 1217–1228.

Sheue C. R., Sarafis V., Kiew R., Liu H. Y., Salino A., Kuo-Huang L. L., Yang Y. P., Tsai C. C., Lin C. H., Yong J. W. H. and Ku M. S. B. (2007). Bizonoplast, a unique chloroplast in the epidermal cells of microphylls in the shade plant *Selaginella erythropus* (Selaginellaceae). *American Journal of Botany* 94, 1922–1929.

Sheue C. R., Liu J. W., Ho J. F., Yao A. W., Wu Y. H., Das S. and Chesson P. (2015). A variation on chloroplast development: the bizonoplast and photosynthetic efficiency in the deep-shade plant *Selaginella erythropus*. *American Journal of Botany* 102, 500–511.

Shimakawa G. and Miyake C. (2018) Oxidation of P700 ensures robust photosynthesis. *Frontiers in Plant Science*, 9, 1617.

Sun H., Zhang S.-B., Liu T. and Wuang W. (2020) Decreased photosystem II activity facilitates acclimation to fluctuating light in the understory plant *Paris polyphylla*. *Biochimica et Biophysica Acta - Bionergetics* 1861, 148135.

Terashima I., Hanba Y.T., Tazoe Y., Vyas P. and Yano S. (2006) Irradiance and phenotype: comparative eco-development of sun and shade leaves in relation to photosynthetic CO_2 diffusion. *Journal of Experimental Botany* 57, 343–354.

Tosens T., Nishida K., Gago J., Coopman R.E., Cabrera H.M., Carriquí M., Laanisto L., Morales L., Nadal M., Rojas R., Talts E., Tomas M., Hanba Y., Niinemets Ü. and Flexas J. (2016) The photosynthetic

capacity in 35 ferns and fern allies: mesophyll CO_2 diffusion as a key trait. *New Phytologist* 209, 1576–1590.

Valdespino I. A. (2015) Novelties in *Selaginella* (Selaginellaceae – Lycopodiophyta), with emphasis on Brazilian species. *PhytoKeys* 57, 93–133.

Valentini R., Epron D., De Angelis P., Matteucci G. and Dreyer E. (1995). In situ estimation of net CO_2 assimilation, photosynthetic electron flow and photorespiration in Turkey oak (*Quercus cerris* L.) leaves: diurnal cycles under different levels of water supply. *Plant, Cell and Environment* 18, 631–640.

Veromann-Jürgenson L.-L., Tosens T., Laanisto L. and Niinemets Ü. (2017) Extremely thick cell walls and low mesophyll conductance: welcome to the world of ancient living!. *Journal of Experimental Botany* 68, 1639–1653.

Veromann-Jürgenson L.-L., Brodribb T.J., Niinemets Ü. and Tosens T. (2020) Variability in the chloroplast area lining the intercellular airspace and cell walls drives mesophyll conductance in gymnosperms. *Journal of Experimental Botany*, eraa231, https://doi.org/10.1093/jxb/eraa231.

Walker A. P., Beckerman A. P., Gu L., Kattge J., Cernusak L. A., Domingues T. F., Scales J. C., Wohlfahrt G, Wullschleger S. D. and Woodward F. I. (2014) The relationship of leaf photosynthetic traits – V_{cmax} and J_{max} – to leaf nitrogen, leaf phosphorus, and specific leaf area: a meta-analysis and modeling study. *Ecology and Evolution* 4, 3218–3235.

Weststrand S. and Korall P. (2016) A subgeneric classification of *Selaginella* (Selaginellaceae). *American Journal of Botany* 103, 2160– 2169.

Xiong D, Douthe C. and Flexas J. (2018) Differential coordination of stomatal conductance, mesophyll conductance, and leaf hydraulic conductance in response to changing light across species. *Plant, Cell and Environment* 41, 436–450.

Youguang Y. and Tan B. C. (2013) The non-functional stomata on the leaf margin of *Selaginella*. *Philippine Journal of Science* 142, 245-248.

Živčak M., Brestič M., Balatova Z., Drevenakova P., Olsovska K., Kalaji H. M., Yang X. and Allakhverdiev S. I. (2013) Photosynthetic electron transport and specific photoprotective responses in wheat leaves under drought stress. *Photosynthesis Research* 117, 529–546.

TABLES

Table 1. Parameters calculated from light-response curves for *Selaginella martensii* grown under extreme shade (L), intermediate shade (M) and full sunlight (H). The plants were analysed at constant *Ca*=400 μmol mol^{-1}. The reported PSII quantum yields were calculated from fluorescence parameters at *I*=400 μmol photons m^{-2} s^{-1}, corresponding to saturated photosynthesis. The rates of day respiration (R_d), maximum net assimilation (A_{max}), assimilation quantum yield (*k*), light compensation point (*LCP*), and irradiance of saturation (I_{sat}) were calculated after *A*-light curve fitting. The values are expressed as the means ± SE (*N*=4-6). Different letters indicate a statistically significant difference according to ANOVA and Tukey's post hoc test (*P*<0.05).

	L	**M**	**H**
F_V/F_M	0.777 ± 0.003[a]	0.788 ± 0.002[b]	0.800 ± 0.003[c]
Y(PSII)	0.088 ± 0.008[a]	0.143 ± 0.011[ab]	0.194 ± 0.028[b]
Y(NO)	0.203 ± 0.010[a]	0.208 ± 0.005[a]	0.169 ± 0.011[b]
Y(NPQ)	0.709 ± 0.017[a]	0.649 ± 0.013[a]	0.636 ± 0.032[a]
PQ	0.43 ± 0.03[a]	0.69 ± 0. 05[a]	1.15 ± 0.16[b]
NPQ	3.53± 0.27[a]	3.14 ± 0.13[a]	3.83 ± 0.42[a]
R_d [μmol CO_2 m^{-2} s^{-1}]	0.41 ± 0.12[a]	0.41 ± 0.10[a]	0.51 ± 0.12[a]
A_{max} [μmol CO_2 m^{-2} s^{-1}]	1.54 ± 0.26[a]	2.68 ± 0.24[b]	3.43 ± 0.55[b]
k [μmol CO_2 μmol^{-1} photons]	0.0468 ± 0.0107[a]	0.0214 ± 0.0033[b]	0.0125 ± 0.0023[b]
LCP [μmol photons m^{-2} s^{-1}]	5.6 ± 1.7[a]	6.6 ± 1.0[a]	11.9 ± 2.4[b]
I_{sat} [μmol photons m^{-2} s^{-1}]	80 ± 14[a]	168 ± 26[ab]	286 ± 50[b]

Table 2. Morphometric parameters related to stomata in *Selaginella martensii* grown under extreme shade (L), intermediate shade (M) and full sunlight (H). The stomata were counted in freshly cut leaves observed under a bright field light microscope. The measurements of single stomata properties were performed during observations using a scanning electron microscope. The values are expressed as the means ± SE of *N* determinations.

	L	**M**	**H**	*N*
Microphyll area [mm^2]	6.50 ± 0.53^{a}	5.89 ± 0.31^{ab}	4.97 ± 0.20^{b}	16
Stomatal density [mm^{-2}]	16.0 ± 1.0^{a}	16.6 ± 0.6^{a}	29.5± 5.4^{b}	12
Stomatal area [μm^2]	503 ± 14^{a}	538 ± 14^{a}	706 ± 20^{b}	18-23
Stomatal aperture [μm]	14.5 ± 0.4^{a}	16.5 ± 0.4^{b}	18.3 ± 0.6^{c}	18-23
Total stomatal aperture length per microphyll area unit [$\mu m\ mm^{-2}$]	232	274	540	

Table 3. Microphyll anatomical parameters in *Selaginella martensii* grown under extreme shade (L), intermediate shade (M) and full sunlight (H). The measured parameters were microphyll thickness T_{leaf}, fraction of mesophyll occupied by intercellular air spaces f_{IAS}, relative chloroplast surface area exposed to intercellular air spaces S_C/S, cell wall thickness T_{cw}, and chloroplast thickness T_{chl}. The values are expressed as the means ± SE of *N* replicates obtained by bright field light microscopy or by transmission electron microscopy for T_{cw}.

	L	**M**	**H**	*N*
f_{IAS} [unitless]	29.9±2.5[a]	27.7±3.0[a]	34.9±2.9[a]	6-7
S_C/S [unitless]	1.13±0.08[a]	1.66±0.06[b]	2.24±0.10[c]	6-7
T_{cw} [nm]	178.9±5.9[a]	167.2±4.6[ab]	162.1±2.8[b]	15
T_{chl} [µm]	9.90±0.41[a]	7.43±0.27[b]	8.31±0.31[c]	48-63

Table 4. Comparison between the plasticity index for selected parameters in seed plants and the corresponding variation in *Selaginella martensii* acclimated to contrasting light regimes from deep shade to full sunlight. The plasticity index in seed plants is reported from Poorter *et al*. (2019) and is the ratio between the highest and lowest value retrieved in their literature meta-analysis. For *S. martensii*, the ratio is similarly calculated between the highest and lowest value measured in our study. F_V/F_M, maximum diurnal quantum yield of PSII; A_{max}, maximum photosynthetic rate on a leaf area basis under saturating light; V_{Cmax}, maximum carboxylation capacity by RuBisCO on a leaf area basis; J_{max}, maximum rate of electron transport for RuBP regeneration.

	Plasticity index in seed plants (from Poorter *et al*., 2019)	**Max/Min in *Selaginella martensii***
F_V/F_M	1.2	1.0
A_{max}	2.2	2.2
V_{Cmax}	2.9	1.6
J_{max}/V_{Cmax}	1.1	1.3
Stomatal conductance	2.2	2.2
Stomatal density	1.8	1.8

FIGURE LEGENDS

Figure 1. Photosynthetic parameters in the lycophyte *Selaginella martensii* increase following long-term light acclimation (extreme shade, L; medium shade, M; high light, H). (A) Representative curves of assimilation (*A*) as a function of the intercellular CO_2 concentration (C_i) recorded at a saturating irradiance of 800 μmol photons m^{-2} s^{-1}. (B) In vivo carboxylation rate by RuBisCO (V_{Cmax}), maximum electron flow used for regeneration of RuBP (J_{max}) and their ratio J_{max}/V_{Cmax}. The values are expressed as the means of *N*=4 (L, H) or 5 plants (M); the error bars indicate SE. ANOVA yielded $P<0.01$ for V_{Cmax} and $P<10^{-4}$ for J_{max}. Significant differences with $P<0.05$ after Tukey's post hoc comparison among L, M, and H plants are indicated by different lowercase letters for V_{Cmax} and different uppercase letters for J_{max}.

Figure 2. Relative importance of CO_2 diffusional path changes in the microphyll of the lycophyte *Selaginella martensii* following long-term light acclimation (extreme shade, L; medium shade, M; high light, H). The values are expressed as the means of *N*=4 (L, H) or 5 plants (M); the error bars indicate SE. For all parameters, ANOVA yielded $P<0.05$ and post hoc Tukey's test was performed. (A) Comparative stomatal conductance (g_s), mesophyll conductance (g_m) and their ratio g_m/g_s. Significant differences among L, M, and H plants are indicated by different lowercase letters for g_s and different uppercase letters for g_m. (B) Total CO_2 conductance g_t. Significant differences are indicated with different lowercase letters. (C) Estimated CO_2 concentration inside the chloroplast (C_c) at an atmospheric CO_2 concentration of 400 μmol mol^{-1} or under conditions of maximum g_m. Significant differences among L, M, and H plants are indicated by different lowercase letters for C_c at 400 μmol mol^{-1} and different uppercase letters for C_c at maximum g_m.

Figure 3. Microscopy examinations of microphylls in the lycophyte *Selaginella martensii* following long-term light acclimation to extreme shade, medium shade or high light). (A-C) Scanning electron microscopy views of stomatal fields at the level of the leaf midrib; note the apparent increasing stomatal density along the light regime gradient. (D-F) Scanning electron microscopy of individual

stomata exemplifying the increase in stoma size and aperture length along the light regime gradient. (G-I) Light microscopy of microphyll semithin sections stained with toluidine blue; in the upper epidermal cells, the shape of the giant chloroplast changes depending on the light regime, increasing its concavity and, thus, its surface exposed to mesophyll air spaces from extreme shade to high light. (J-L) Transmission electron micrographs of the cell wall in the upper epidermal cells at positions interposed between the chloroplast (right side) and mesophyll air space; a slight, though visible, reduction in cell thickness occurs along the gradient in the light regime. For each row of panels, the magnification is the same and the corresponding scale bar is reported.

Figure 4. Comparative limitation analysis in the lycophyte *Selaginella martensii* following long-term light acclimation to extreme shade (L), medium shade (M) or high light (H). The total limitation of photosynthesis is 1 and results from the sum of its components: stomatal conductance limitation (l_s), mesophyll conductance limitation (l_m), and biochemical limitations, including both electron transport and carboxylation (l_b). The values are expressed as the means of N=4 (L, H) or 5 plants (M); the error bars indicate SE. The probabilities resulting from ANOVA are reported in the graph. Significant differences emerging after post hoc Tukey's comparison among L, M, and H plants are indicated by different lowercase letters for l_m and by different uppercase letters for l_b.

Figure 5. Analysis of electron flows in the lycophyte *Selaginella martensii* following long-term light acclimation to extreme shade (L), medium shade (M) or high light (H). (A) Linear electron flow J_{PSII}. (B) Partitioning of linear electron flow to photosynthetic carbon fixation (J_C), photorespiration (J_O), and alternative electron sinks (J_A). (C) Electron flow ratio between photosynthesis and photorespiration. (D) Relative electron flow to alternative sinks. The values are expressed as the means of N=4 (L, H) or 6 plants (M); the error bars indicate SE. The probabilities resulting from ANOVA are reported in each graph; different letters in (A) indicate a significant difference as evaluated by Tukey's post hoc test with P<0.05.

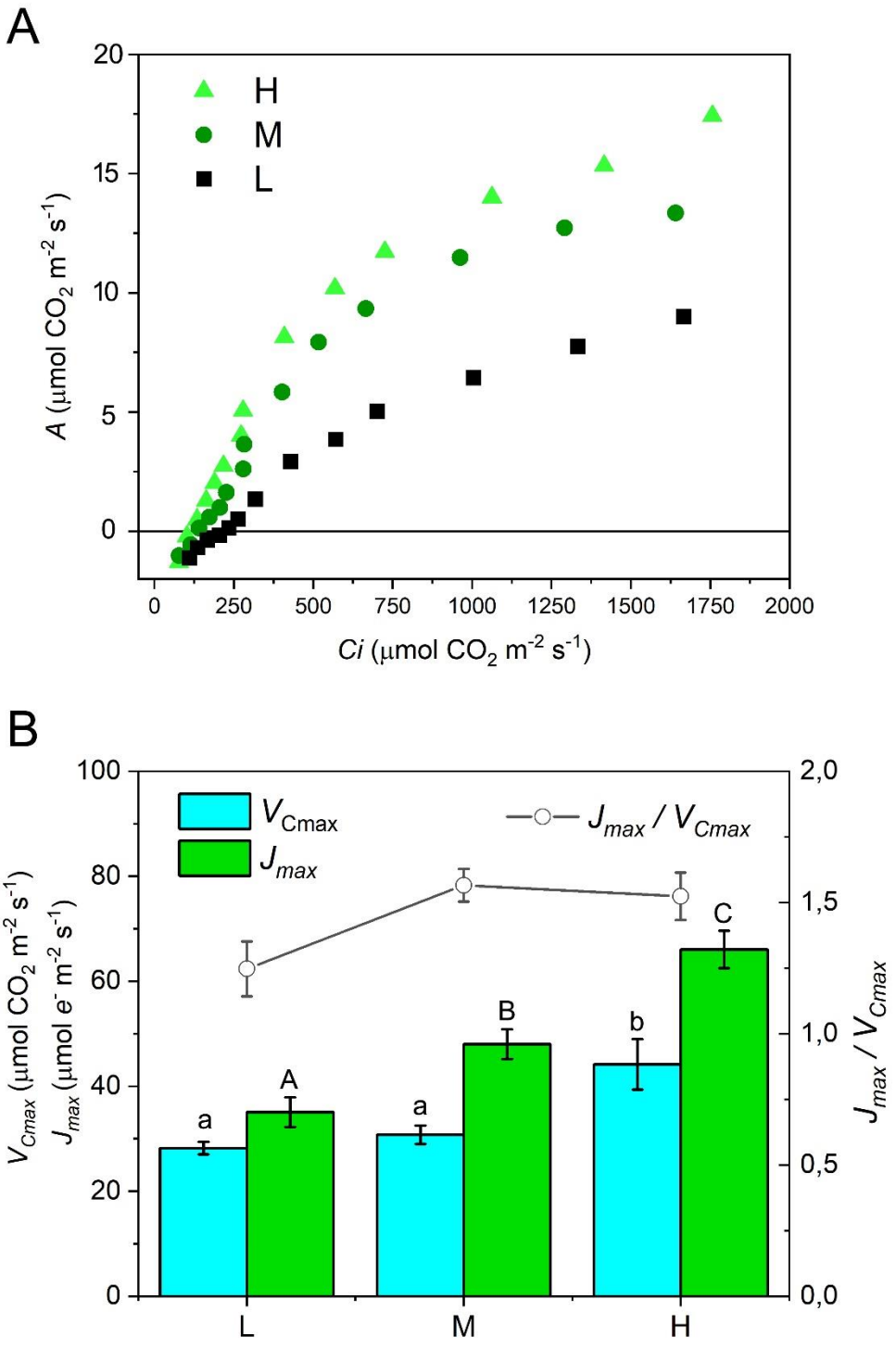
A
H
M
L
A (µmol CO2 m-2 s-1)
Ci (µmol CO2 m-2 s-1)
B
VCmax
Jmax
Jmax / VCmax
VCmax (µmol CO2 m-2 s-1)
Jmax (µmol e- m-2 s-1)
Jmax / VCmax
a
A
a
B
b
C
L
M
H

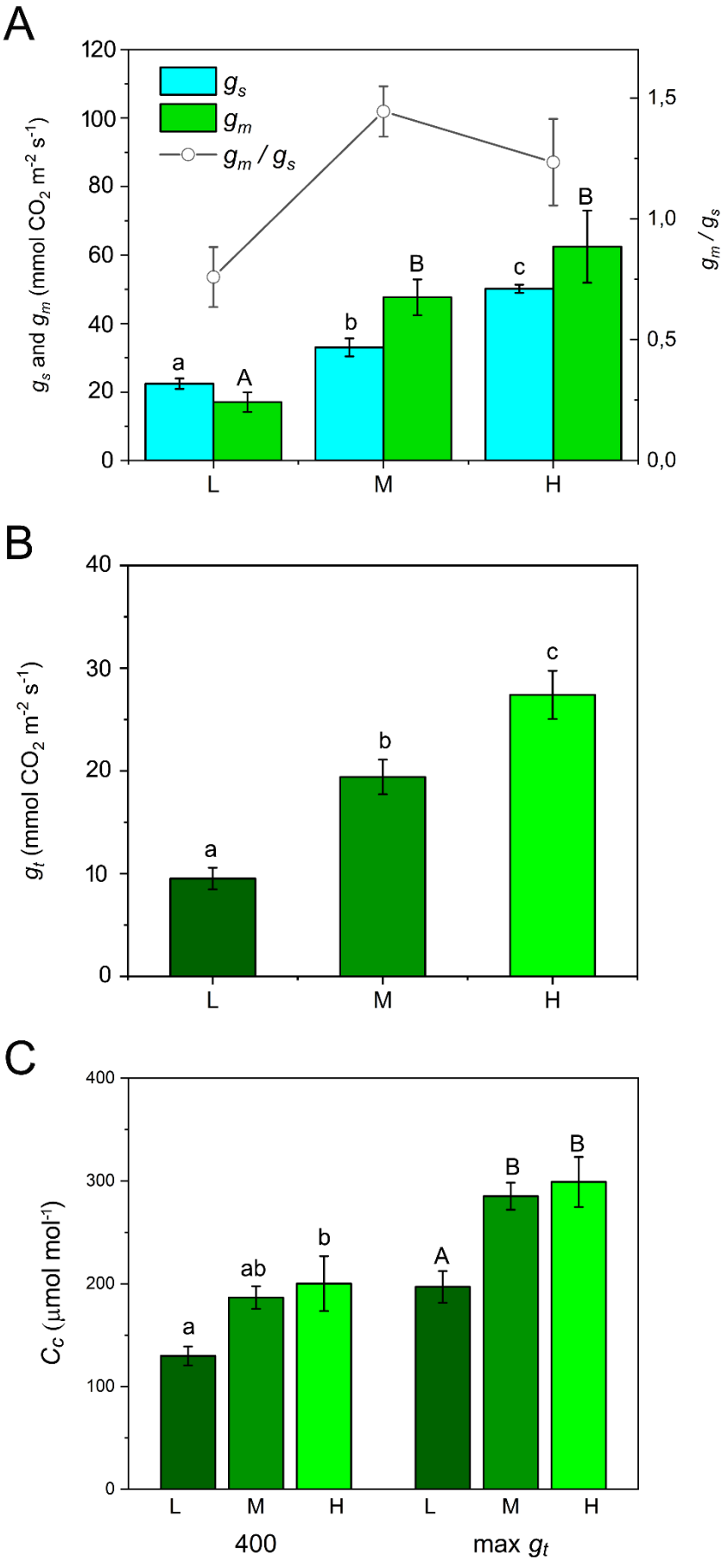
A
120
100
80
60
40
20
0
1,5
1,0
0,5
0,0
g_s
g_m
g_m / g_s
g_s and g_m (mmol CO_2 m^{-2} s^{-1})
g_m / g_s
a
A
b
B
c
B
L
M
H
B
40
30
20
10
0
g_t (mmol CO_2 m^{-2} s^{-1})
a
b
c
L
M
H
C
400
300
200
100
0
C_c (µmol mol^{-1})
a
ab
b
A
B
B
L
M
H
L
M
H
400
max g_t

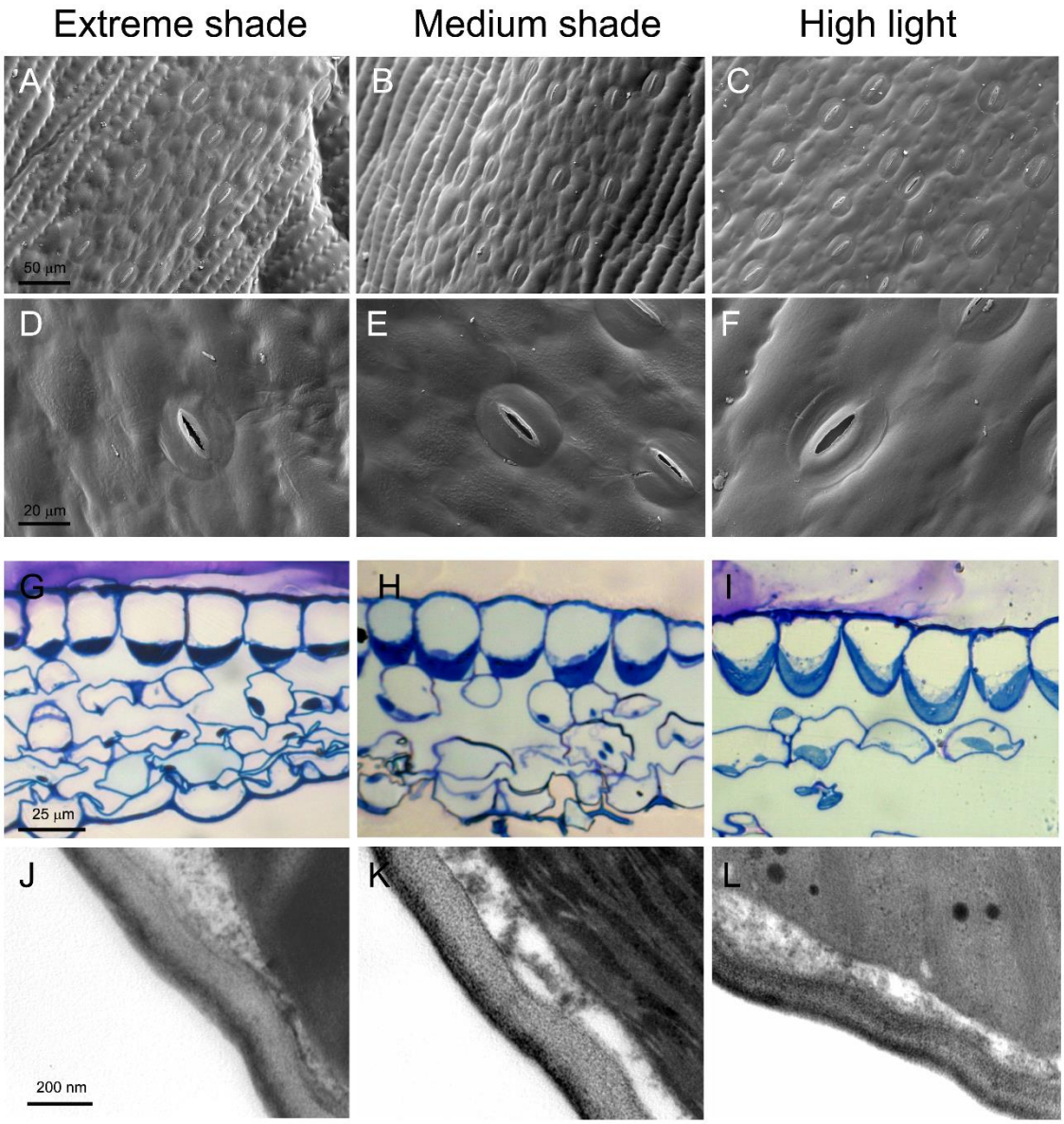
Extreme shade
Medium shade
High light
A
B
C
50 µm
D
E
F
20 µm
G
H
I
25 µm
J
K
L
200 nm

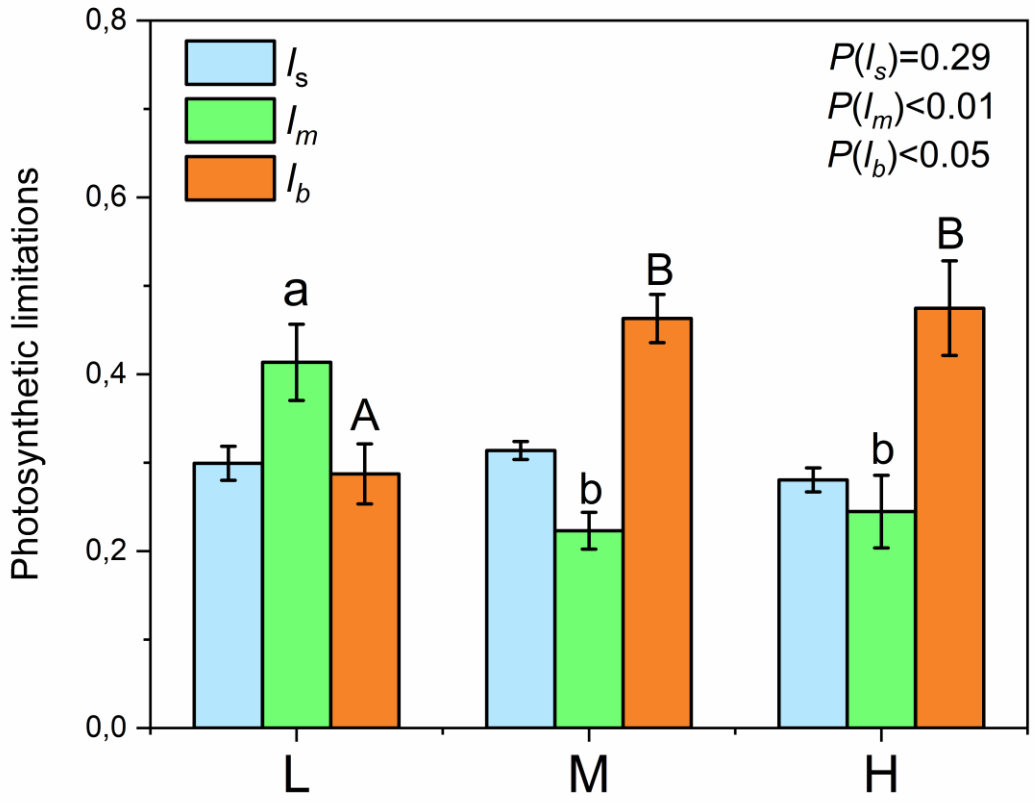
Photosynthetic limitations
0,8
0,6
0,4
0,2
0,0
I_s
I_m
I_b
$P(I_s)$=0.29
$P(I_m)$<0.01
$P(I_b)$<0.05
a
A
b
B
b
B
L
M
H

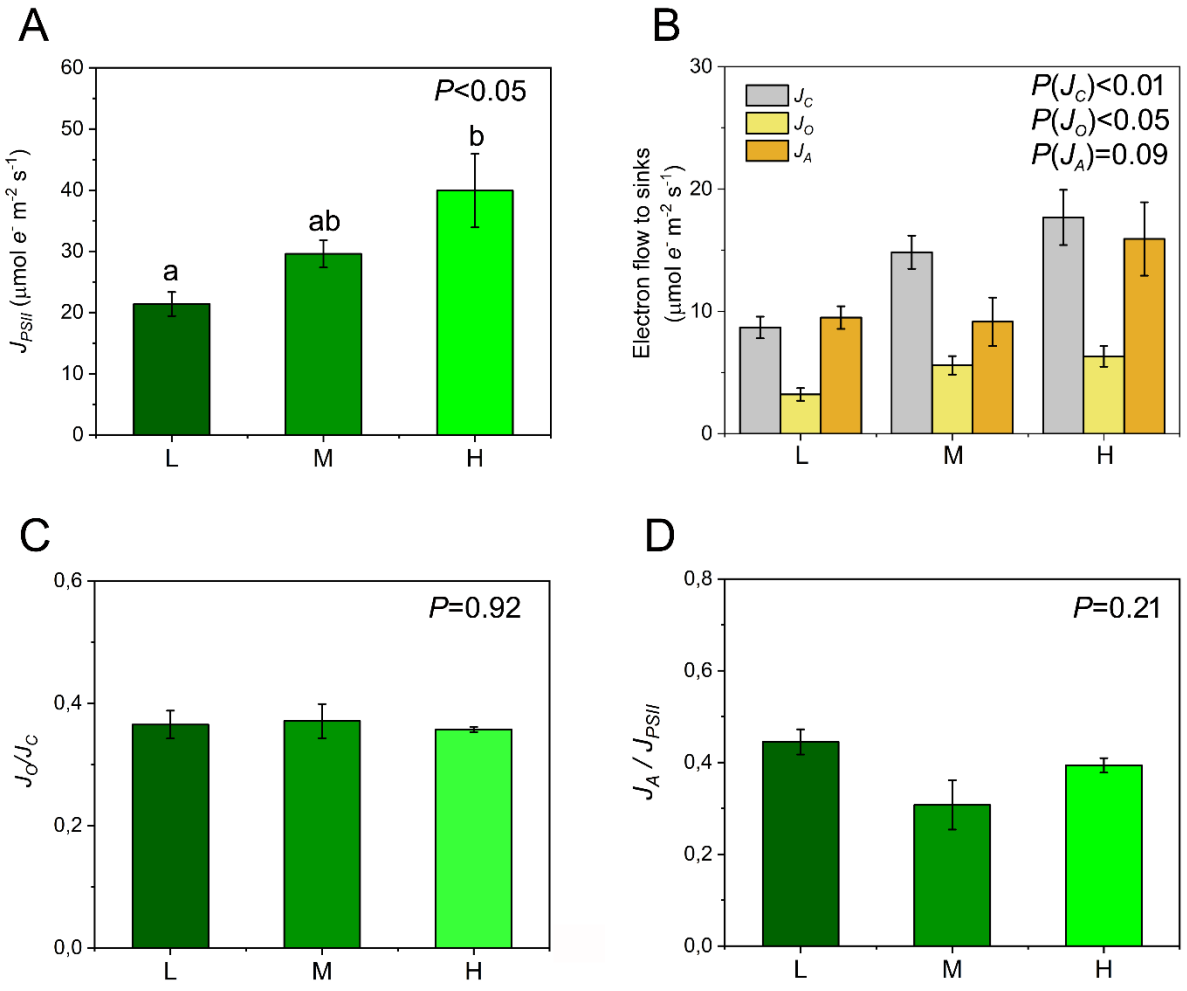
A
B
C
D
P<0.05
a
ab
b
L
M
H
J_{PSII} (µmol e^- m^{-2} s^{-1})
Electron flow to sinks (µmol e^- m^{-2} s^{-1})
J_C
J_O
J_A
$P(J_C)$<0.01
$P(J_O)$<0.05
$P(J_A)$=0.09
J_O/J_C
P=0.92
J_A / J_{PSII}
P=0.21